Journal of Electronic Imaging 11(2), 195–205 (April 2002).

Prediction of the texture visibility of color halftone patterns

Muge Wang
Sipix Imaging, Inc.
1075 Montague Expressway
Milpitas, California 95035

Kevin J. Parker
University of Rochester
Department of Electrical and Computer Engineering
Rochester, New York 14627
E-mail: parker@ece.rochester.edu

Abstract. *We propose a metric to predict the visibility of color halftone textures. This metric is represented by the critical viewing distance below which the halftone textures can be discriminated. It is intended to be used in the evaluation of the texture visibility of uniform color halftone patterns, which plays an important role in halftone design and optimization. The metric utilizes the visual threshold versus intensity function and contrast sensitivity functions for luminance and chrominance. To verify the metric, the texture visibility was determined experimentally using a psychovisual experiment. The critical viewing distances determined by the experiment and those predicted by the metric were compared, and a good correlation was achieved. The results have shown that the metric is capable of predicting the visibility over a wide range of texture characteristics.* © *2002 SPIE and IS&T.* [DOI: 10.1117/1.1455010]

1 Introduction

Halftoning design and optimization largely relies on the quantitative measurement of the quality of halftone patterns. For example, the blue noise mask (BNM)[1,2] algorithm requires a criterion by which to control the optimization process of halftone patterns for each level. Perhaps the most widely used image quality metric or error metric in halftone quality assessment is the frequency weighted mean square error (FWMSE). For most of the algorithms that generate blue noise dithering matrices, quality control is realized by minimizing the FWMSE either explicitly (in the frequency domain) or implicitly (in the image domain). A review of algorithms for generating blue noise masks was given by Spaulding *et al.*[3] In their paper, they introduced the different error metrics that were chosen as stopping criteria for the optimization process of generating halftone patterns. Most of them belong to the category of FWMSE. In other work, the FWMSE has also been applied to halftone pattern quality evaluation. Comparisons of different halftone techniques have been performed using the FWMSE.[4–6]

Other halftone quality metrics include multichannel model and S-CIELAB metrics. The multichannel model is distinguished from the single model in that a number of independent filters that span the frequency domain are used. The idea of utilizing a multichannel model in quality evaluation is very similar to that of the FWMSE. The difference is that the single channel visual model in the FWMSE is replaced by a multiple channel visual model that accounts for the frequency and orientation selectivity of the human eye. One of the multiple channel models is the visible differences predictor (VDP) proposed by Daly,[7] which is primarily an image fidelity metric. Other studies related to the evaluation of halftone quality using multiple channel models can be found in the work of Mitsa *et al.*, of Farrell *et al.*, and others.[8,9] Compared to the single channel model, the multichannel model is more computationally intensive. Another metric that can be utilized in halftone quality evaluation is S-CIELAB[10] which is spatially extended CIELAB color space.[11] Proposed by Zhang and Wandell, this metric is suitable for images that are not comprised of large uniform areas and it can be used to evaluate the visibility of halftone textures.[12]

Despite the wide use of FWMSE in halftoning applications, it does have limitations. One is that it can only be applied to gray scale halftoning. The second limitation is that the FWMSE only provides an error represented by a number, and this does not give a clue as to the visual response caused by this error.

The proposal of a metric in this paper is motivated by the need for an automatic and objective measurement of halftone texture visibility, particularly at the threshold level. The contribution of the metric is that the calculated error values of images are linked with perceptual visual responses by the human visual threshold function. More specifically, this metric is capable of predicting the critical

Paper JEI 001007 received Feb. 12, 2001; revised manuscript received Aug. 24, 2001; accepted for publication Oct. 4, 2001.
1017-9909/2002/$15.00 © 2002 SPIE and IS&T.

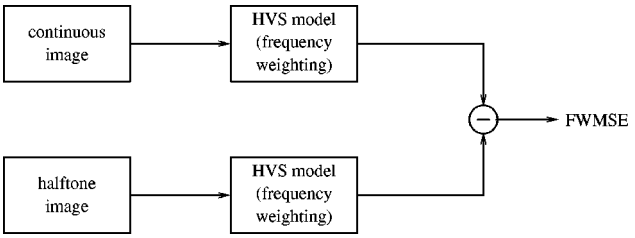

Fig. 1 Illustration of how to calculate the FWMSE.

viewing distance or displaying resolution so that the halftone textures of a uniform color pattern appear to be just noticeable, or whether or not a uniform color halftone pattern is visible to the human eye under a given viewing condition. Designed as a quality metric at the threshold level, this metric is useful for halftone design in which a stopping criterion is often required for optimization of each gray level, as well as evaluation of the quality and for a comparison among different halftone techniques.

In Sec. 1.1, the definition of the FWMSE is given and its limitations are illustrated. In Sec. 1.2, the idea that led to the development of this metric is presented.

1.1 *FWMSE*

FWMSE is the widely used quality metric in many imaging applications. How to calculate the FWMSE is illustrated in Fig. 1. In halftoning, the frequency weighted errors between a continuous image and its halftoned version are evaluated. The frequency factors used in the evaluation are the frequency responses of the human visual system. Thus, larger weighting factors are used for the frequencies to which the eye is more sensitive, and smaller weighting factors are used for the frequencies to which the eye is less sensitive.

Evaluation of the FWMSE is normally conducted in the discrete frequency domain. It is illustrated by the example of finding the FWMSE of a uniform halftone pattern with gray level g_0. Let $g(m,n)$ denote the halftone pattern in the image domain, $G(k,l)$ denote its discrete Fourier transform (DFT), and $H(k,l)$ be the human visual system (HVS) function represented in discrete frequency (f_k, f_l), and the size of the pattern be $N \times N$. In this example, the original continuous image is a uniform gray patch with gray level of g_0, and thus its DFT is $g_0 \delta_{00}$. Then the discrete Fourier transform of the error image $e(m,n)$, $E(k,l)$ is

$$E(k,l) = G(k,l)H(k,l) - g_0 \delta_{00}. \tag{1}$$

In the image domain, Eq. (1) becomes

$$e(m,n) = \mathcal{F}^{-}\{G(k,l)H(k,l)\} - g_0, \tag{2}$$

where $\mathcal{F}^{-1}$ is the inverse discrete Fourier transform. According to Parseval's theorem, the MSE between the continuous image and its halftone version can be thus calculated by

$$\text{FWMSE} = \frac{1}{N^2} \sum_{k=0}^{N-1} \sum_{l=0}^{N-1} |G(k,l)|^2 |H(k,l)|^2. \tag{3}$$

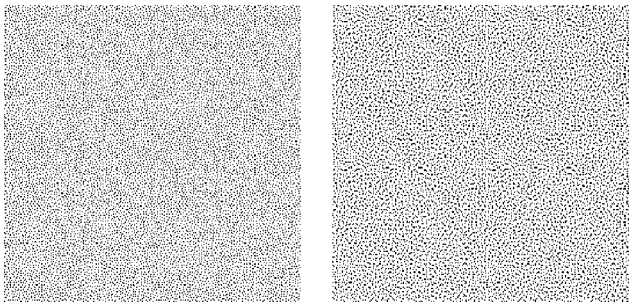

Fig. 2 Two gray patches with $g = 211$. Left: Blue noise pattern 1. Right: Blue noise pattern 2.

In the above equation, note that the DC term of $(k,l) = (0,0)$ should be excluded from the summation.

The FWMSE metric employs the characteristics of human visual sensitivity as a function of spatial frequency to model the visual process, and thus it provides more meaningful results than the nonweighted MSE. Despite the meaningful results, its simplicity and generality, the FWMSE sometimes is not clear or can produce confusing results. Specifically, let us consider the two blue noise halftone patterns illustrated in Fig. 2. The two halftone patterns have the same gray levels but they were generated by different processes, and thus they have different appearances. In order to calculate their FWMSE, we must specify the print resolution and viewing distance.[13] Suppose the print resolution for the two patterns is 300 dpi. When viewed from 12 in. away, the FWMSEs of the two patterns are

$$\text{FWMSE}_{b1} = 0.0816,$$

$$\text{FWMSE}_{b2} = 0.1079.$$

When viewed from 24 in. away, the FWMSEs of the two patterns are

$$\text{FWMSE}_{b1} = 0.0234,$$

$$\text{FWMSE}_{b2} = 0.0216.$$

By comparing the results of the FWMSEs, we conclude that the rankings by FWMSE may give different answers when the viewing distance changes. In this example, when the viewing distance is set to 12 in., the FWMSE of pattern 1 is less than that of pattern 2, indicating that pattern 1 will result in smaller visual errors than pattern 2; however, when the viewing distance is set to 24 in., the FWMSE of pattern 1 is larger than that of pattern 2, which is opposite to the situation of a viewing distance of 12 in. Thus, by assigning different viewing distances, the FWMSE provides different results. However, there is no visual interpretation of the result given by the FWMSE. This example shows that, although the FWMSE is capable of indicating the relative quality of an image, it cannot relate the error to visual experience.

1.2 *Metric for Color Halftone Texture Visibility*

A halftone is intended to produce the illusion of continuous images from binary output states, so the visibility of undes-

ired halftone textures is an essential factor of the quality of halftone patterns. Since the task of halftoning is to produce the illusion of a continuous image from a limited number of output levels with minimal visual errors, we would then expect the ideal implementation of a halftone is to generate a nearly perfect continuous-like image without perceivable halftone texture and artifacts. From practical experience, the viewer will typically view the halftone images at varying distances. Thus, the quality can be judged based on the halftone texture visibility with respect to the viewing distance. The concern for producing perfect halftone patterns will lead to questions such as, at a typical printing resolution, at what distance will the halftone textures become ''invisible,'' or at a given viewing distance and resolution, is the texture of the halftone pattern perceivable? Thus a metric is needed to define the critical conditions, generally speaking, the viewing distance or resolution, under which the halftone texture is just perceivable. Represented by the critical viewing distance or resolution, this metric actually is an indicator of the halftone pattern's quality in terms of visibility at the threshold level. The smaller the distance, the higher the quality, and vice versa.

Yu *et al.*[14] proposed such a halftone texture visibility metric for uniform color halftone patches. It combines a progressively low-pass filtering operation with a texture detection model based on Weber's law,[14] which will be introduced in Sec. 2. In the model, the detection threshold was related to the average intensity of the halftone patterns. Then they developed a psychovisual experiment to measure the texture visibility by the distance at which an observer can see the halftone texture of a color halftone patch with fixed resolution. The experimentally measured texture visibility was compared with the cut-off frequency calculated by the metric. Most of the result correlated well with the metric, however, there was a group of green patterns that produced inconsistent results compared to the metric. We noticed that the average luminance of the green patterns (about 12 cd/m^2) was somewhat lower than that of the other patterns (from 29 to 47 cd/m^2). One explanation of this is that Weber's law is not an appropriate model by which to define the detection threshold for halftone patterns, which contain a high frequency modulated content.

Therefore, we wanted to reconsider the validity of applying Weber's law to this particular application. Extensive research has been carried out to study the visual threshold with regard to the intensity.[15–19] It was pointed out that human vision exhibited different behavior under different conditions, e.g., the background intensity, size, spatial and temporal frequency of the stimulus, etc. We utilized these analyses in the halftone quality applications and proposed a new texture visibility metric based on the threshold versus intensity functions.

The conditions under which the visual threshold law is valid is reviewed and an appropriate model is chosen for the halftone application. Other relevant psychological topics of contrast sensitivity functions of achromatic and chromatic stimuli are presented. Then a metric is proposed to predict the distance at which the halftone texture can be just distinguished. The psychological background that accounts for the development of the metric is a combination of the visual threshold function and the contrast sensitivity function. Then, a psychological experiment is addressed. The experiment was developed to subjectively determine the visibility of color halftone patterns generated by several halftone schemes. The results show that a good correlation between the distances measured and the distances predicted was achieved.

2 Study of the Visual Threshold

Our aim here in Sec. 2 is to provide the background of the threshold versus background intensity under different conditions. Our intention is to choose an appropriate relationship and to utilize it in our halftone quality metric rather than to explore the mechanisms behind visual behavior. Much research has been carried out to study human visual behavior at the just noticeable threshold level. Experiments were used to find visual thresholds at various conditions and the relationship between the threshold and intensity.[15,17] Threshold being dependent on the background intensity is referred to as the threshold versus intensity (TVI) function.

The different characteristics of the TVI function indicate the consequences of different mechanisms in the visual perception process. Three types of visual behavior have been discovered under normal viewing conditions.

1. At low intensity levels, the curve is close to being a flat line, indicating that the visual threshold is independent of the background intensity. This segment is called the absolute threshold because an absolute value takes effect regardless of the change in intensity. The threshold function can be represented by

$$\Delta I = \text{const}, \tag{4}$$

   where ΔI denotes the threshold.

2. At midintensity levels, on a log–log scale, the curve has a slope of 1/2. This means that the threshold is related to the background intensity as

$$\frac{\Delta I}{I_0^{1/2}} = \text{const}, \tag{5}$$

   where ΔI denotes the threshold and I_0 denotes the background intensity. This relationship is also called the de Vries–Rose law or square root law because the threshold is a constant fraction of the square root of the background illuminance. A theoretical equation can be derived to explain this relationship by modeling the number of photons absorbed by the photoreceptors in the retina as a random variable with Poisson distribution.[18,19]

3. At higher intensity levels, on a log–log scale, the slope of the curve is close to 1. This means that the threshold is proportional to the background illuminance:

$$\frac{\Delta I}{I_0} = \text{const}. \tag{6}$$

This relationship, that is, that the change in stimulus intensity that can just be discriminated is a constant fraction of the intensity of the stimulus, is usually referred to as We-

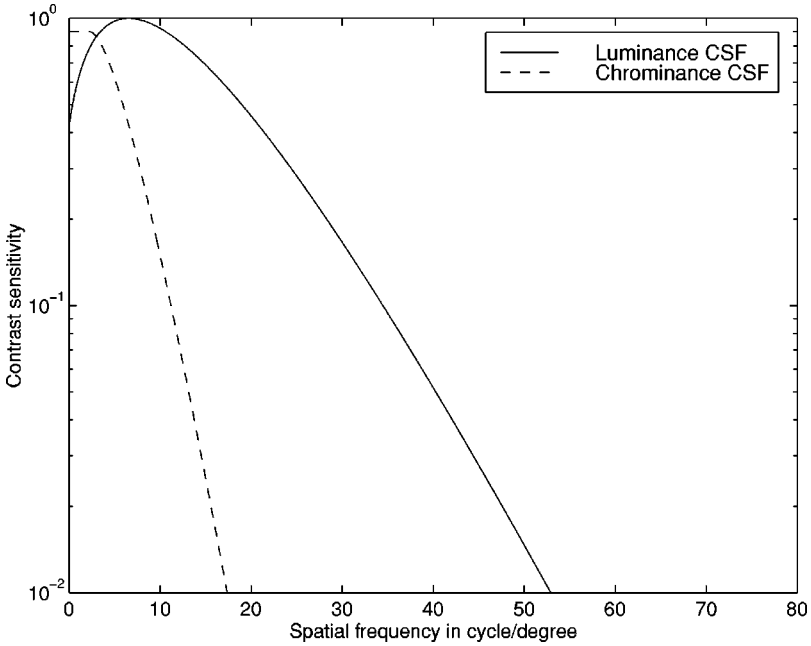

Fig. 3 Illustration of the luminance and chrominance CSF. The luminance CSF and the chrominance CSF are represented by the solid line and the dashed line, respectively.

ber's law. This law is named after E. H. Weber, the German physiologist, who discovered the relationship that applies to many types of sensations of human sensing organs.[20] It is believed that Weber's law is a result of some more complicated mechanisms. Some theoretical interpretations have been developed to explore the biological mechanisms of this visual phenomenon.[21]

The absolute threshold, de Vries–Rose law and Weber's law apply under different circumstances. The transition from one stage to another stage is not abrupt. Additionally, there are no deterministic breakpoints to separate these stages, because the discrimination threshold critically depends on the stimulus physical parameters, such as the intensity, size, duration, and wavelength composition of the target and background. In general, de Vries–Rose law holds for targets of small size, with high spatial frequency, or a short duration, whereas Weber's law holds for targets of large size, with low spatial frequency, or a long duration.[21] The transition intensity I from the de Vries–Rose range to Weber's range shifts toward higher luminance for higher spatial frequencies.

As mentioned in Sec. 1, we intend to develop a quality metric at the threshold level. The TVI function provides us with a psychological basis on which to define the detection threshold of a uniform color halftone patch, in which the average luminance (or the luminance of the original continuous color patch) can be considered as the background intensity. The question is which stage best characterizes the visual perception of halftone textures at the threshold level. Since blue noise patterns have most of their energy located in the high frequency range and have little energy at the low frequency band, it is reasonable to assume that the square root law will apply to the stimuli of blue noise patterns. In addition, recent work by Peli *et al.*[22] showed that the square root law was confirmed as stimulus luminance up to 50 cd/m^2 with spatial frequency of 16 cycles per degree (cpd). Their results were consistent with the results reported by van Nes and Bouman.[15] The luminance levels we examined in our experiment (Sec. 5) fell into the range between the two works, so we adopt the de Vries–Rose law to define the threshold in our model in Sec. 4.

3 Contrast Sensitivity Function for Achromatic and Chromatic Gratings

3.1 *Contrast Sensitivity Function*

In many imaging applications, the HVS model is approximated by the contrast sensitivity function (CSF). From the opponent color theory, chromatic perception can be separated into red or green (RG) and yellow or blue (YB), and achromatic perception into white or black (WK).[23] The human visual system is more sensitive to changes of luminance than to changes of chrominance with regard to spatial frequency. The behavior of the sensitivity to luminance modulation can be modeled by a band pass filter, which has a drop-off slope at very low spatial frequencies. The behavior of the sensitivity to chrominance modulation can be modeled by a low-pass filter which has a much lower cutoff frequency than the CSF of luminance. An illustration of the different characteristics of CSF for achromatic and chromatic gratings is shown in Fig. 3, where the solid line indicates the luminance CSF and the dashed line indicates the chrominance CSF.

3.2 *HVS Model for Achromatic and Chromatic Gratings*

The formulas of the HVS model for luminance $H_l(r)$ and chrominance $H_c(r)$, respectively, used in this paper are expressed by the following equations:

$$H_l(f_r) = 2.2(0.192 + 0.114 f_r)\exp[-(0.114 f_r)^{1.1}], \qquad (7)$$

$$H_c(f_r)=\begin{cases} 1.98(0.192+0.342\,f_r)\exp[-(0.342\,f_r)^{1.1}], \\ \quad \text{if } f_r>f_{\max}, \\ 0.9 \quad \text{otherwise}, \end{cases} \tag{8}$$

where f_r in Eqs. (7) and (8) denotes the radial spatial frequency in units of cycle/deg, and $f_{\max}$ in Eq. (8) is the frequency in which $H_c(f_r)$ reaches its maximal value.

The two HVS models are illustrated in Fig. 3. Equation (7) is the formula defined by Sullivan *et al.*[13,24] without modification of the low-pass term. Equation (8) is similar in form to Eq. (7), except that f_r is scaled by a factor of 3 and the magnitude is scaled by a factor of 0.9. Thus, the chrominance CSF is a low-pass function and it has a steeper drop-off slope than the luminance CSF. The two scale factors were chosen primarily based on the consideration that the two formulas should be consistent with the luminance and chrominance sensitivities measured by other researchers.[25–27] In their results, the low-pass and narrower band properties of the chrominance modulation discrimination were verified, and the corresponding CSF was measured.

In order to convert the discrete frequency to frequency in cycle/deg, knowledge of the viewing distance d (in units of in.) and print resolution P is required. Assuming that the support of the DFT of the image is $N\times N$, and that (k,l) is the position in the frequency domain, f_k and f_l can then be calculated by

$$f_k=\frac{\pi k d P}{N180}, \tag{9}$$

and

$$f_l=\frac{\pi l d P}{N180}. \tag{10}$$

The radial frequency is thus given by

$$f_r=\frac{\sqrt{f_k^2+f_l^2}}{s}, \tag{11}$$

where s is a scale factor. It is added in Eq. (11) in order to compensate for the decrease in sensitivity at angles other than those in horizontal and vertical directions. s is expressed as a function of the angle θ:[24]

$$s(\theta)=\frac{1-\omega}{2}\cos(4\theta)+\frac{1+\omega}{2}, \tag{12}$$

where

$$\theta=\arctan\left(\frac{f_l}{f_k}\right), \tag{13}$$

and ω is chosen empirically as 0.7.

4 Metric to Predict the Visibility Distance

In Secs. 2 and 3, properties of the visual threshold and contrast sensitivity were introduced. Here in Sec. 4, these properties are utilized to derive the texture visibility metric. The de Vries–Rose law depicts the relationship between the detectable threshold and the background intensity. For a uniform color halftone patch, the background intensity I can be considered as the average luminance of the halftone patch. The threshold in the TVI function is referred to as the amount of intensity increase of the target versus a uniform background. To utilize de Vries–Rose law, an approximate threshold which can best represent the concept in the TVI needs to be defined. In our model, ΔI is estimated by the total error from all achromatic and chromatic channels, in which the error from each channel is defined as the standard deviation of the HVS filtered channel. Because the metric is primarily applied at the threshold level, it is fairly reasonable to take the standard deviation as the effective change in intensity.

We use a uniform color halftone patch to develop this metric. The halftone image was converted to opponent color space and divided into luminance and chrominance channels. The CSF function is converted to a digital filter to model visual behavior in observing an image at a particular distance in the discrete frequency domain using Eq. (11). Then the luminance and chrominance information is treated separately according to the characteristics of each. The visual threshold from de Vries–Rose law is applied to quantize the visual results to ''on'' or ''off,'' which indicates whether the pattern is either ''visible'' or ''invisible'' under the given viewing condition. Then the critical distance which causes a just noticeable difference is calculated by an iterative process. The flow chart for this is illustrated in Fig. 4, and the procedure can be outlined as follows.

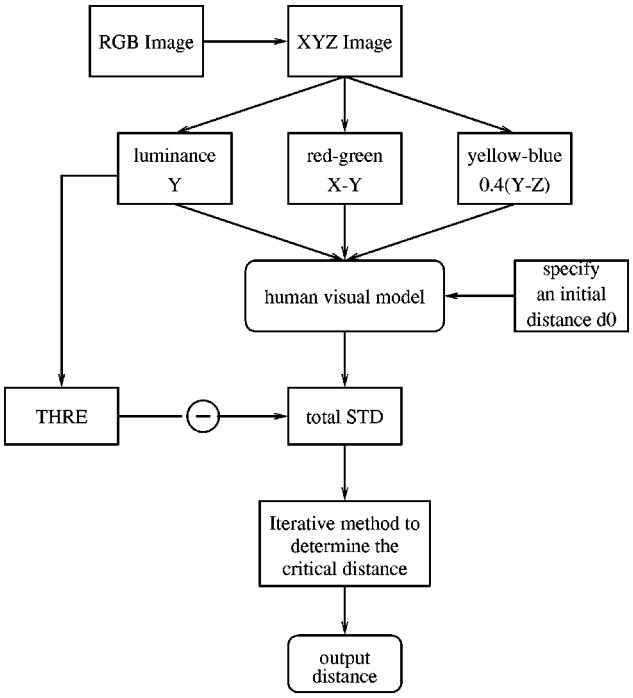

Fig. 4 Flow chart showing how to calculate the critical distance.

1. Start with the displayed image represented in the device's RGB space.
2. Convert the representation in the device's RGB space to the device's independent XYZ space.
   The conversion was implemented by the matrix operation

$$\begin{pmatrix} X \\ Y \\ Z \end{pmatrix} = T \times \begin{pmatrix} \mathrm{R} \\ \mathrm{G} \\ \mathrm{B} \end{pmatrix}, \tag{14}$$

   where T is defined in Eq. (19) and it was obtained from monitor characterization.
3. The image represented in XYZ space was separated to one achromatic image $y(m,n)$ (the luminance channels) and two chromatic images $o_1(m,n)$ (red/green) and $o_2(m,n)$ (yellow/blue). The method to separate the three channels was based on Eq. (15). The Y component represents the white/black of the image. The two chrominance, red/green (R/G) and yellow/blue (Y/B) can be represented by[23]

$$\begin{cases} \mathrm{W}-\mathrm{K}=Y, \\ \mathrm{R}-\mathrm{G}=X-Y, \\ \mathrm{Y}-\mathrm{B}=0.4(Y-Z). \end{cases} \tag{15}$$

   Thus the colorimetric image was divided into three channels, with one representing the luminant information and the other two representing two chrominant information. Then the three channels are passed through the visual response filters which approximate, in a simple linear sense, the human visual system.
4. Define the visual threshold. The threshold is specified according to de Vries–Rose law:

$$t=c*(Y)^{1/2}, \tag{16}$$

   where the constant c was chosen as 1/40 and Y is the luminance channel which can be calculated from Eq. (15).
5. Specify an initial distance d_0. d_0 can be assigned to an arbitrary value.
6. Calculate the standard deviation STD_0 of the image which is being observed at the current distance. The method by which to find the error in the observed image will be addressed later in Eq. (18).
7. Compare the STD_0 to threshold t in Eq. (16). Increase d_0 if STD_0 is larger than t, and decrease d_0 if STD_0 is smaller than t.
8. Use the iterative approach to determine the critical distance d, where the resulting error is equal to threshold t in Eq. (16).

The method by which to calculate the total error of the observed image is outlined below and the flow chart for it can be found in Fig. 5.

1. Calculate the HVS model of luminance and chrominance in the discrete frequency domain at the current distance.

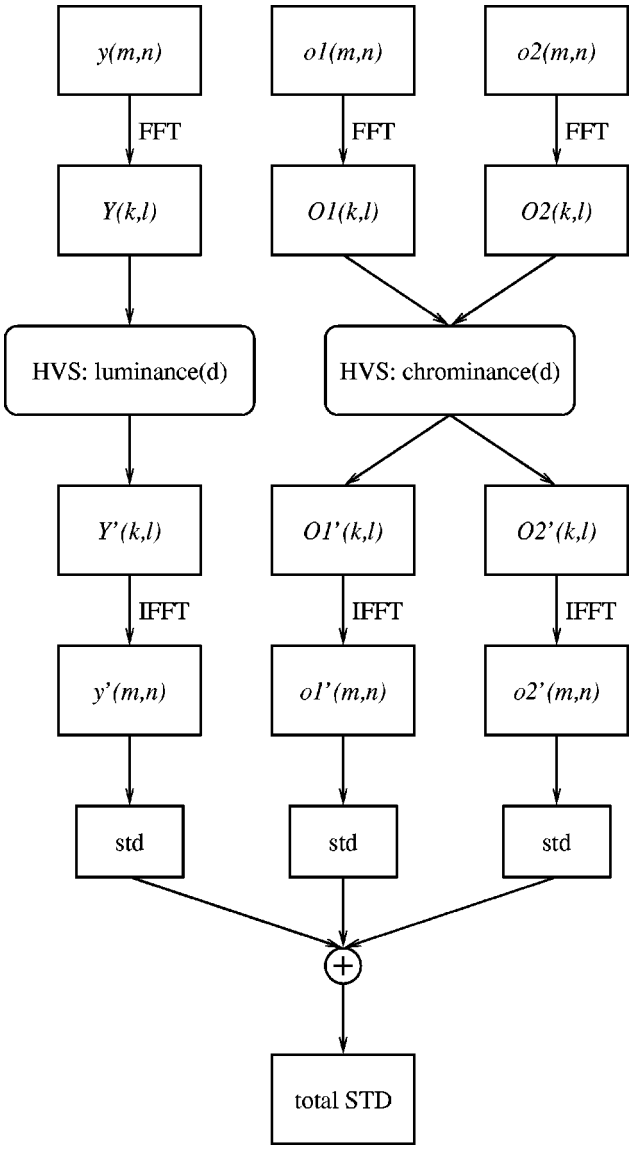

Fig. 5 Flow chart showing how to calculate the total error of the color image.

2. Obtain the discrete Fourier transform $Y(k,l)$, $O_1(k,l)$ and $O_2(k,l)$ of $y(m,n)$, $o_1(m,n)$, and $o_2(m,n)$, respectively. Apply the corresponding filters to the images in the Fourier domain.

$$\begin{cases} Y'(k,l)=Y(k,l)\otimes H_l(k,l), \\ O_1'(k,l)=O_1(k,l)\otimes H_c(k,l), \\ O_2'(k,l)=O_2(k,l)\otimes H_c(k,l), \end{cases} \tag{17}$$

   where $\otimes$ is the element multiplication operator, and $Y'(k,l)$, $O_1'(k,l)$, and $O_2'(k,l)$ are the filtered patterns.
3. Take the inverse discrete Fourier transform of $Y'(k,l)$, $O_1'(k,l)$, and $O_2'(k,l)$. The results are blurred images $y'(m,n)$, $o_1'(m,n)$, and $o_2'(m,n)$ in the image domain.
4. Find the sum of the standard deviation of the three images

$$\mathrm{STD} = \mathrm{std}(y') + \mathrm{std}(o_1') + \mathrm{std}(o_2'), \tag{18}$$

where STD is the observed error in the image.

5 Experiment

We now introduce an experiment to determine the visibility of halftone patterns subjectively. As explained in Sec. 1, we will examine the critical viewing conditions that cause marginal perception experimentally. Since continuously adjusting the display resolution is impractical, we used a fixed resolution to present the stimuli and changed the viewing distances instead.

5.1 *Apparatus*

A 21 in. SGI monitor was used to display the stimuli. The monitor was characterized by a tristimulus colorimeter. The luminance of the white point is 55.2 cd/m^2. The tristimulus values (X, Y, Z) of the RGB phosphors were measured. The matrix T to convert from the device's RGB space to the XYZ space was obtained from the following characterization:

$$T = \begin{pmatrix} 0.4070 & 0.3042 & 0.2269 \\ 0.2256 & 0.6927 & 0.0817 \\ 0.0270 & 0.1424 & 1.2043 \end{pmatrix}. \tag{19}$$

Since all the target patterns in this experiment are halftone patterns, the phosphors were at a status of either ''on'' or ''off,'' so no gamma correction is needed. The advantage of using displayed images as stimuli is that it is easy to program and control the display sequences.

5.2 *Stimuli*

All the stimuli used in this experiment were color halftone patches. To reduce the effect of the modulation transfer function (MTF) of the monitor, each pixel was duplicated twice in both the horizontal and vertical directions, and the effective display resolution was 43 dpi. The images were 512×512 pixels, and all the stimuli were 15 cm$\times$15 cm squares. The stimuli were displayed in the center of a uniform medium gray background. During the experiment, only one stimulus was presented on the screen each time. The experiment was conducted under conventional office lighting with fluorescent illumination and without sunlight or visible glare on the display. Observers viewed the stimuli binocularly.

The experimental stimuli were chosen as the halftone images of uniform color patches of different color. The uniform patches were halftoned with different techniques so they exhibit different texture characteristics. Four techniques were used to generate the color halftone patterns. They are Bayer's dithering,[28] scalar error diffusion,[29] single blue noise mask (dot on dot), and mutually exclusive blue noise masks (dot off dot).[30,31] For the Bayer's dithering, the same Bayer's dithering matrix is used for all RGB planes, so there is no offset or rotation between them. Scalar error diffusion is a technique whereby each color plane is halftoned with the standard error diffusion individually and then combined with other color planes. The dot-on-dot technique applies a single blue noise mask on all the color planes without shifting or rotating them. The dot-off-dot technique applies a set of specifically designed masks to each of the color planes. The masks are derived from a set of mutually exclusive seed patterns, therefore, this technique can achieve higher spatial frequency than the dot-on-dot technique. We chose these four schemes because they have some interesting characteristics. Bayer's dithering generates periodic patterns which are optimal at some levels but objectionable at some other levels. The other three techniques all generate blue noise halftones, but their differences can be quite distinct in some situations.

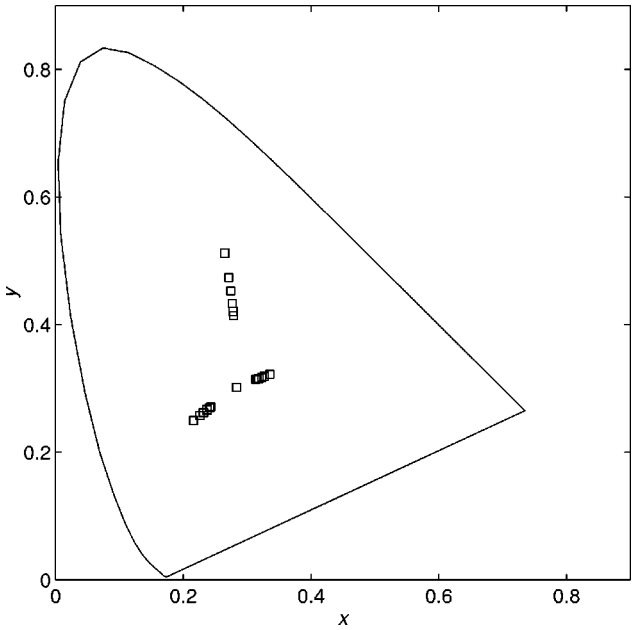

Fig. 6 Chromaticity values of the test patterns plotted in the CIE 1931 chromaticity diagram.

Gray and three sets of common colors (sky blue, skin color, and green) were chosen as the colors for the original uniform patches. For each set of color patches, they had about the same saturation and hue values, but their luminance values varied. The luminance values of the three sets of color images were approximately 15%, 25%, 35%, 50%, 65%, and 75% of the white point of the monitor, which was 66 cd/m^2. Thus all the images covered a range of luminance as well as various values of chromaticity. The values of the chromaticity of the stimuli are plotted in Fig. 6. The luminance of these patches was from about 8 to 50 cd/m^2. There was a total 25 colors, and each of them was halftoned by four techniques, so there were 100 color halftone images.

5.3 *Procedure*

The procedure for the experiment basically followed the procedure in Yu *et al.*'s experiment.[14] The subjects first stood far away from the monitor (about 23 ft). Under controlled viewing conditions, at this distance all the halftone patterns were perceived as uniform patches. Then the subjects walked slowly toward the monitor until they could discriminate the textures of the halftone patterns. The subjects were allowed to move back and forth slightly to de-

Table 1 Mean results of all the observers. The distances are in units of ft.

Pattern	Dot-on-dot technique	Dot-off-dot technique	Error diffusion	Bayer dithering
15% gray	18.9	16.4	13.1	13.7
25% gray	18.3	16.7	15.2	7.07
35% gray	16.1	15.0	12.2	15.6
50% gray	16.3	14.1	13.4	4.75
65% gray	14.3	13.4	12.4	12.1
75% gray	13.8	13.2	11.3	7.47
85% gray	13.6	11.5	10.1	15.1
15% blue	16.8	16.2	12.7	18.0
25% blue	16.7	16.3	13.0	15.9
35% blue	16.5	15.4	12.8	17.2
50% blue	14.3	14.6	11.1	16.0
65% blue	13.9	12.9	11.1	14.3
75% blue	12.9	12.5	10.2	15.9
15% skin	16.7	16.5	13.0	19.5
25% skin	16.1	15.9	12.6	13.8
35% skin	15.9	14.9	13.0	14.3
50% skin	15.7	14.6	9.98	16.0
65% skin	14.7	13.0	11.1	12.0
75% skin	13.0	13.2	11.0	16.3
15% green	16.6	15.0	15.5	17.1
25% green	15.4	16.2	14.8	16.4
35% green	16.1	15.2	11.2	17.6
50% green	14.3	14.0	10.6	15.4
65% green	14.3	12.7	11.0	13.8
75% green	13.2	11.9	11.9	15.1

termine the best position. The distances at which they were able to just detect the texture of the halftone patterns were recorded.

The whole experiment was divided into four sessions to prevent observer fatigue. In each session one set of color images was used as the stimuli. The four sessions were assigned at different but successive time segments. Each subject took only one session in one time segment. The patterns were presented twice in random order. For each pattern, the difference between the two measurements was calculated promptly. If the error was larger than a predetermined value, the pattern would be displayed one more time in the same session.

5.4 *Results*

Six subjects participated in the experiment. The mean values of all the observers are listed in Table 1. A graphic representation of the results will be given in Figs. 7 and 8 in Sec. 6, where a comparison with the metric defined in Sec. 4 is illustrated. Generally, the error diffusion patterns resulted in overall smallest distances. This means that the error diffusion patterns had the least amount of visibility among all the types of patterns. The dot-off-dot (mutually exclusive masks) outperformed the dot-on-dot patterns, especially for the gray patches. For the Bayer's patterns at optimal levels, for example, at 25%, 50%, and 75%, the visibility was very low. However, for other levels of Bayer's patterns, the visibility was very high, particularly for some color patterns.

6 Discussion

6.1 *Correlation Between the Metric and Experimental Results*

A threshold factor of 1/40 was used as factor c in Eq. (16). This fraction is in the range of a typical factor for perception by eye.[20,32] From the calculations and a comparison with the experimental data, a factor of 1/40 was found to be the most suitable to define the visual threshold factor. In this paper, the intensities were scaled according to the reference white point on the monitor, which was normalized to 1. The threshold is a fraction of the square root of the intensity, so the factor should be multiplied by a scale factor if another intensity unit is used or if the dynamic range of the display or printing device is changed. There are other two factors, both for the chrominance CSF, that were determined empirically. One is the factor of spatial frequency f_r (3 in this case), and the other is the factor of the magnitude of the CSF (0.9 in this case). The factors were determined to ensure that the two CSF functions possess the fundamental characteristics of achromatic and chromatic vision and that they are consistent with the CSF depicted in related

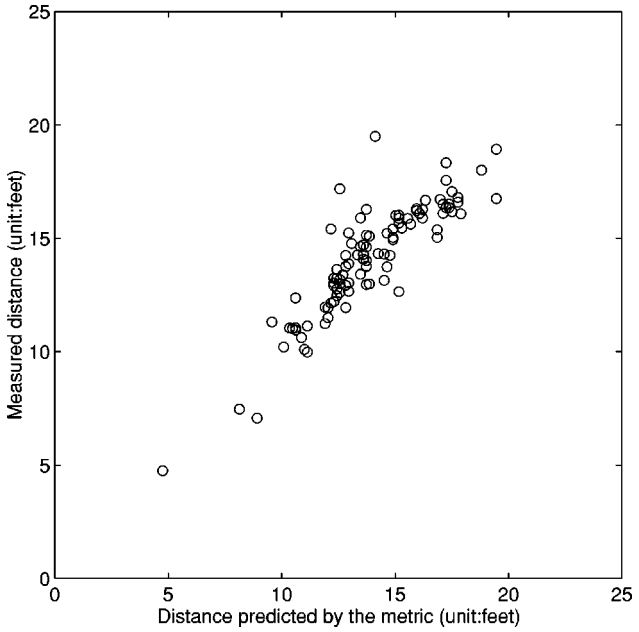

Fig. 7 Mean experimental results vs the distance from the metric.

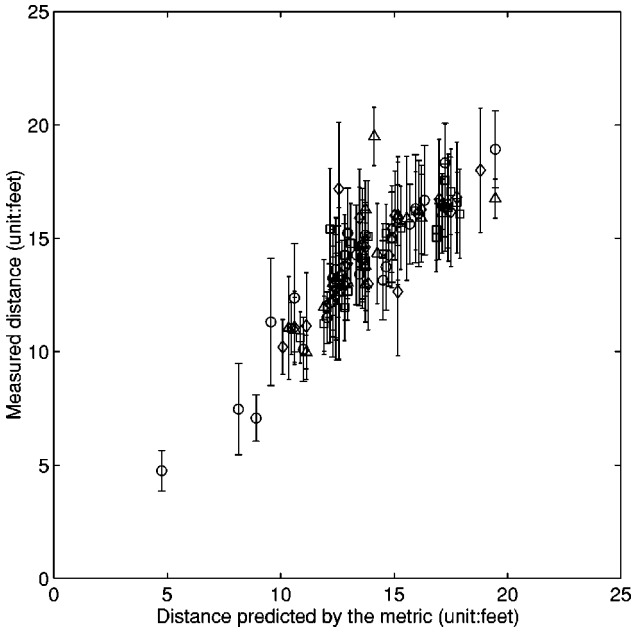

Fig. 8 Average and standard deviations of the experimental results and the distance from the metric.

work.[25–27] Also, the two factors were adjusted within a small range during metric development, and they had no large effect on the results of the metric predicted so the CSF again is found to provide a useful description of the achromatic and chromatic characteristics of the visual system in this case.

It can be seen that a strong similarity exists between the procedure for the experiment and the algorithm to derive the critical viewing distance. The algorithm can be considered as simulating the process of walking back and forth and adjusting to the position at which the observer can barely discriminate the texture. Changing the viewing distance causes a shift of the HVS model in the discrete frequency domain, and thus causes a change in frequency content that could be captured by the eye. As the observer walks closer to the monitor, the spatial variation of the pattern increases, and the critical distance is that where the total error just exceeds the visual threshold.

The experimental results and the distances calculated by the proposed metric are illustrated in Figs. 7 and 8. The x axes in Figs. 7 and 8 are the distances predicted by the metric, and the y axes are the experimental results. Figure 7 illustrates the mean values for all the observers versus the predicted values. Figure 8 is the same as Fig. 7 except that standard deviations are included. By inspecting Figs. 7 and 8, it can be seen that a good linear correlation exists between the experimental results and the metrics. The linear correlation coefficient of the data is $r=0.88$.

The standard deviation of the images was used as the average of the increment in intensity versus the uniform background. Kaiser and Boynton have discussed the issue of interaction between opponent color channels[33] and they specified the empirical rule for the interaction as:

$$F=[|r-g|^n+|y-b|^n]^{1/n}, \tag{20}$$

where F is the overall effect caused by the R-G channel and Y-B channel, and n can be any positive integer. When $n=1$, the interaction is the sum of the two channels. This is the rule we applied in the calculation of the total errors in Eq. (18). If vector summation (corresponding to $n=2$) is used, because the luminance errors dominate the total errors, the effect of chrominance errors is practically eliminated. In the case in which chrominance information is ignored by choosing $n=2$, the correlation coefficient of the data is $r=0.84$ instead of $r=0.88$ when $n=1$. Although the difference seems to not be significant, it is not sufficient to model the perception of color halftone patches with luminance only, so scalar summation is used to estimate the overall error in our model. For image quality metrics, there are other techniques with which to evaluate the overall error from all the channels according to the specific applications. For example, Daly employed the method of probability summation to calculate the overall influence of errors from all the bands in the algorithm of visible differences predictor.[7]

6.2 *Discussions on the Experiment*

At the average distance, which was about 14 ft, the stimuli subtended an angle of 2°. The experiment is not a fixed distance experiment, so adjustment of the viewing distances caused changes in focal length. The 5% and 95% values of the distances measured in the experiment are 10 and 17 ft, which is equal to 3 and 5.1 m, respectively. The change in focal length between these two distances is about 0.14 D. This is a small number, so the effect of accommodation can be ignored.

6.3 *Application of the Metric*

This experiment is not intended to study the strict conditions of the visual threshold function of halftone patterns. It emphasizes that the metric developed by this model can faithfully predict the texture visibility of color halftone pat-

terns. The intensity levels tested in this experiment were from about 8 to 50 cd/m^2. For hardcopy prints illuminated by typical office lighting, the luminance may be beyond the range tested using the cathode ray tube (CRT) display. For intensity higher than 50 cd/m^2 or lower than 8 cd/m^2, the validity of the de Vries–Rose law is not verified, nor is it guaranteed. Our suggestion is to use a smoothly changed threshold function that combines the de Vries–Rose law and Weber's law when necessary. However, for a small dynamic range, e.g., one from 50 to 70 cd/m^2, the difference in threshold determined by de Vries–Rose's law and by Weber's law is not significant, so de Vries–Rose law can be extended to the application at intensity levels higher than 50 cd/m^2.

The halftone patterns generated by different techniques usually have some distinct characteristics. For example, Bayer's dithering generates periodic patterns. These patterns are optimal at some levels, whereas the patterns may be quite visible for other levels. The patterns generated by error diffusion and the blue noise mask also have some different features, although they are both blue noise generators. Despite the various halftone characteristics, our metric is capable of producing good predictions for all cases. Although the patterns selected in the experiment may not represent halftone techniques in general, the approach is independent of the texture characteristics and thus can apply to various halftone techniques.

Increasing the viewing distance will have approximately the same effect as increasing the print or display resolution in the case for which the perceived halftone images under the condition that there are no significant dot gain or frequency modulation effects. This is because the scaling factor of converting discrete frequency to continuous frequency is the product of the print resolution and viewing distance. In our experiment, the quality is evaluated by the critical distance. It can also be used to find out the critical resolution if a typical viewing distance is assumed. If this model is used under given conditions, such as a given viewing distance and display resolution, a single number output will be produced to indicate whether the texture visibility is under or above the threshold.

This metric can be a guide to evaluating the quality of the resulting halftone patterns. Assessment of texture visibility of halftone patterns is usually based on an assessment of uniform halftone patches. Comparison of the halftone images of a gray ramp is a basic and important evaluation in most halftone evaluations. A blue noise dither matrix is actually composed of binary halftone images at all the gray levels. The overall quality of the blue noise mask can be obtained by inspecting the critical distances of all the levels. For example, Bayer's dithering is proved to be optimal at some specific levels but it does not necessarily indicate that the Bayer's matrix is optimal as a whole. The metric can be applied directly to quality assessment of halftone patterns of solid patches, and thus can aid in blue noise mask design.

7 Conclusion

It this paper, we proposed a simple but fundamental measurement of color halftone texture visibility at the threshold level. Represented by the critical viewing distance at which the halftone textures can just be discriminated, this metric has been shown to correlate well with the experimental results. The potential application of this metric is not limited to a comparison of the quality of uniform color halftone patches. As was mentioned earlier in this paper, it can be incorporated into halftone algorithms as an objective quality assessment in addition to the FWMSE, or as a criterion for simultaneous optimization of the blue noise mask.

References

1. T. Mitsa and K. J. Parker, ''Digital halftoning using a blue noise mask,'' *J. Opt. Soc. Am. A* **9**, 1920–1929 (1992).
2. K. J. Parker and T. Mitsa, ''Method and apparatus for halftone rendering of a gray scale image using blue noise mask,'' U.S. Patent No. 5, 111, 310 assigned to Research Technologies Corporation (1992).
3. K. E. Spaulding, R. L. Miller, and J. Schildkraut, ''Methods for generating blue-noise dither matrices for digital halftoning,'' *J. Electron. Imaging* **6**(2), 208–230 (1997).
4. T. Mitsa, ''Evaluation of halftone techniques using psychovisual testing and quantitative quality measures,'' in *Human Vision, Visual Processing, and Digital Display III*, *Proc. SPIE* **1666**, 177–187 (1992).
5. Q. Lin, ''Halftone image quality analysis based on a human vision model,'' in *Human Vision, Visual Processing, and Digital Display IV*, *Proc. SPIE* **1913**, 378–389 (1993).
6. Q. Yu, K. J. Parker, K. Spaulding, and R. Miller, ''Digital multitoning with overmodulation for smooth texture transition,'' *J. Electron. Imaging* **8**(3), 311–321 (1999).
7. S. Daly, ''The visible differences predictor: An algorithm for the assessment of image fidelity,'' *Digital Images and Human Vision*, pp. 179–206, MIT Press, Cambridge, MA (1993).
8. T. Mitsa, K. L. Varkur, and J. R. Alford, ''Frequency-channel-based visual models as quatitative quality measures in halftoning,'' *Human Vision, Visual Processing, and Digital Display IV*, *Proc. SPIE* **1913**, 390–401 (1993).
9. J. E. Farrell, X. Zhang, C. J. van den Branden Lambrecht, and D. A. Silverstein, ''Image quality metrics based on single and multi-channel models of visual processing,'' *Proc. IEEE Compcon 97*, pp. 56–60 (1997).
10. X. Zhang and B. A. Wandell, ''A spatial extension of CIELAB for digital color image reproduction,'' *SID Symp. Tech. Dig.* **27**, 731–734 (1997).
11. CIE, Section 4, ''Recommendations concerning uniform color spacing,'' *Colorimetry*, 2nd ed., CIE publication No. 15.2 (1986).
12. X. Zhang, D. A. Silverstein, J. E. Farrell, and B. A. Wandell, ''Color image quality metric S-CIELAB and its application on halftone texture,'' *Proc. IEEE Compcon 97*, pp. 44–48 (1997).
13. J. Sullivan, L. Ray, and R. Miller, ''Design of minimum visual modulation halftone patterns,'' *IEEE Trans. Syst. Man Cybern.* **21**(1), 33–38 (1991).
14. Q. Yu, K. J. Parker, R. Buckley, and V. Klassen, ''A new metric for color halftone visibility,'' in *Recent Progress in Digital Halftoning II*, edited by R. Eschbach, pp. 72–76, Society for Imaging Science and Technology, Springfield, VA (1999).
15. F. L. van Nes and M. A. Bouman, ''Spatial modulation transfer in the human eye,'' *J. Opt. Soc. Am.* **57**(3), 401–406 (1967).
16. H. B. Barlow, ''Optic nerve impulses and Weber's law,'' *Cold Spring Harb Symp. Quant Biol.* **30**, 539–546 (1965).
17. D. H. Kelly, ''Adaptation effects on spatio-temporal sine-wave thresholds,'' *Vision Res.* **12**, 89–101 (1972).
18. H. L. de Vries, ''The quantum character of light and its bearing upon the threshold of vision, the differential sensitivity and acuity of the eye,'' *Physica (Amsterdam)* **10**, 553–564 (1943).
19. A. Rose, ''The sensitivity performance of the human eye on an absolute scale,'' *J. Opt. Soc. Am.* **38**, 196–208 (1948).
20. G. A. Geschelder, *Psychophysics, Method, Theory, and Application*, pp. 2–7, Lawrence Erlbaum Associates, Hillsdale, NJ (1985).
21. M. E. Rudd, ''A neural timing model of visual threshold,'' *J. Math. Psychol.* **40**, 1–29 (1996).
22. E. Peli, L. Arend, and A. T. Labianca, ''Contrast perception across changes in luminance and spatial frequency,'' *J. Opt. Soc. Am. A* **13**(10), 1953–1959 (1996).
23. L. M. Hurvich and D. Jameson, ''Some quantitative aspects of an opponent-colors theory. II. Brightness, saturation and hue in normal and dichromatic vision,'' *J. Opt. Soc. Am.* **45**(8), 602–616 (1955).
24. J. Sullivan, R. Miller, and G. Pios, ''Image halftoning using a visual model in error diffusion,'' *J. Opt. Soc. Am. A* **10**(8), 1714–1724 (1993).
25. G. J. C. van der Horst and M. A. Bouman, ''Spatiotemporal chromaticity discrimination,'' *J. Opt. Soc. Am.* **59**(11), 1482–1488 (1969).
26. E. M. Granger and J. C. Heurtley, ''Visual chromaticity modulation transfer function,'' *J. Opt. Soc. Am.* **63**(9), 73–74 (1973).
27. K. T. Mullen, ''The contrast sensitivity of human colour vision to

red-green and blue-yellow chromatic gratings,'' *J. Physiol.* **359**, 381–400 (1985).
28. B. E. Bayer, ''An optimum method for two-level rendition of continuous-tone pictures,'' *Proc. IEEE Int. Conf. Commun.* (26-11)–(26-15) (1973).
29. R. W. Floyd and L. Steinberg, ''An adaptive algorithm for spatial greyscale,'' *Proc. Soc. Inf. Disp.* **17**(2), 75–77 (1976).
30. M. Wang and K. J. Parker, ''Properties of jointly-blue noise masks and applications to color halftoning,'' *J. Imaging Sci. Technol.* **44**(4), 360–370 (2000).
31. Q. Yu and K. J. Parker, ''Stochastic screen halftoning for electronic imaging devices,'' *J. Visual Commun. Image Represent* **8**(4), 423–440 (1997).
32. P. K. Kaiser and R. M. Boynton, *Human Color Vision*, pp. 196–248, Optical Society of America, Washington, DC (1996).
33. P. K. Kaiser and R. M. Boynton, *Human Color Vision*, pp. 328–330, Optical Society of America, Washington, DC (1996).

Muge Wang received her BS and MS degrees in physics from Tsinghua University, Beijing, China, in 1993 and 1996, respectively. Then she attended the graduate school of the University of Rochester and received her MS and PhD degrees in electrical engineering in 1998 and 2001, respectively. She worked for Eastman Kodak Company during the summer of 1999. She is currently a senior research scientist at Sipix Imaging Inc. Her research interests include digital halftoning, digital image processing, color image processing, and digital video processing.

Kevin J. Parker received his BS degree in engineering science, *summa cum laude*, from SUNY at Buffalo in 1976. Graduate work in electrical engineering was done at MIT, with MS and PhD degrees received in 1978 and 1981, respectively, for work in electrical engineering with a concentration in bioengineering. Dr. Parker is a professor of electrical and computer engineering, radiology, and bioengineering at the University of Rochester where he has held positions since 1981. In 1998, Dr. Parker was named Dean of the School of Engineering and Applied Sciences at the University of Rochester. Dr. Parker has received awards from the National Institute of General Medical Sciences (1979), the Lilly Teaching Endowment (1982), the IBM Supercomputing Competition (1989), the World Federation of Ultrasound in Medicine and Biology (1991), and the Joseph P. Holmes Pioneer Award from the American Institute of Ultrasound in Medicine (AIUM) (1999). He is a member of the IEEE, the Acoustical Society of America (ASA), and the AIUM. He was named a fellow of both the IEEE and the AIUM for his work in medical imaging and of the ASA for his work in acoustics. In addition, he has recently completed a three-year term on the board of governors of the AIUM. Dr. Parker's research interests are in medical imaging, linear and nonlinear acoustics, and digital halftoning.